Proton scattering by ^{206,207,208}Pb at 650 MeV: Phenomenological analysis

A. M. Mack,[1] Norton M. Hintz,[1] D. Cook,[1] M. A. Franey,[1] J. Amann,[2] M. Barlett,[3,*] G. W. Hoffmann,[3] G. Pauletta,[3,†] D. Ciskowski,[3‡] and M. Purcell[3]

[1]*School of Physics and Astronomy, University of Minnesota, Minneapolis, Minnesota 55455*

[2]*Los Alamos National Laboratory, Los Alamos, New Mexico 87545*

[3]*Department of Physics, University of Texas, Austin, Texas 78712*

(Received 19 September 1994)

Elastic and inelastic differential cross sections and analyzing powers are presented for the scattering of 650 MeV protons from ^{206,207,208}Pb. Five phenomenological optical potential sets with comparable χ^2 values are obtained. The volume integrals and root-mean-square (rms) radii of these potential sets are compared with those expected from the impulse approximation. The agreement is close for the imaginary, but not the real central potentials. The potential rms radii are $\sim 3\%$ smaller than those from the impulse approximation indicating a "shrinking" of the effective nuclear density. The inelastic data for ^{206,208}Pb are analyzed using collective transition densities. The results are then compared with electromagnetic matrix elements to obtain neutron-proton transition matrix element ratios. These are in fairly good agreement with earlier determinations and indicate large core polarization contributions to the low-lying "two neutron hole" states in ^{206}Pb.

PACS number(s): 25.40.Cm, 24.10.Ht, 25.40.Ep, 27.80.+w

I. INTRODUCTION

A determination of neutron and proton static and transition densities can be made by a comparison of π^+ and π^- scattering [1,2] or alternately by proton (or other hadronic probes) and electron scattering [3–5]. The Pb isotopes are particularly interesting for proton studies because of the existence of high-quality electron-scattering data [6–10] and the many theoretical predictions for static and transition densities [11–16] which, in general, have been tested only for charge distributions.

We report here experimental results for 650-MeV elastic ^{206,207,208}Pb and inelastic (^{206,208}Pb) proton scattering at the Los Alamos Meson Physics Facility. In a later paper, the inelastic data for ^{207}Pb will be presented. In this paper the elastic results have been analyzed to obtain phenomenological optical potentials. The inelastic data have been studied using the simple collective vibrating potential and vibrating density models. In a recent paper [17], the nonrelativistic impulse approximation has been used with an effective interaction (determined by fitting ^{40}Ca) to extract model-independent ground-state neutron densities from these data.

In a second paper [18], the derived ground-state neutron densities for ^{206,207,208}Pb have been used to obtain constraints on the value of the nuclear compressibility.

In a third paper [19] we have presented a comparison of the inelastic data with theoretical neutron and proton, microscopic transition densities.

Section II is a discussion of experimental methods, Sec. III presents the phenomenological optical potential analysis, and Sec. IV presents the analysis of the inelastic scattering from ^{206,208}Pb to obtain neutron-proton transition matrix element ratios. The results are compared with those from π^+ and π^- scattering for ^{206,208}Pb and earlier electron-hadron determinations for ^{208}Pb. The analysis of the inelastic ^{207}Pb data will appear in a later paper.

II. EXPERIMENTAL METHODS

The experiment was performed at the Los Alamos Meson Physics Facility (LAMPF) using the High Resolution Spectrometer (HRS) [20] and with polarized protons ($P_b \simeq 75$–85%) at 650 MeV. Isotopically enriched targets (92–99 %) in the 150 mg/cm^2 range were employed. An overall energy resolution of $\Delta E \simeq 100$ keV was achieved. The angular range covered was from 4° to 25° in 1.5° steps. Using information from the multiwire drift chambers in the focal plane [21] the data were binned into four 0.5° intervals at each spectrometer angle. At each angle the three targets were interchanged 4–6 times at 10–20 min intervals to average out small systematic errors in the relative 206-207-208 cross sections due to instabilities in beam or detector parameters. The angular resolution was approximately, $\Delta\theta \simeq 0.04°$ and the uncertainty in absolute angle $\delta\theta = \pm 0.02°$.

The data for all three isotopes were corrected for a small angular shift, $\delta\theta$, in the apparent laboratory angle (θ_a) relative to the true angle (θ_t), i.e., $\theta_t = \theta_a + \delta\theta$ where $\delta\theta = 0.1°$. The value of $\delta\theta$ was determined by comparison with an earlier experiment [22] on ^{208}Pb at

*Present address: Applied Research Laboratories, The University of Texas, Austin, TX 78713.

†Present address: Department of Physics, University of Udine, 33100 Udine, UD, Italy.

‡Present address: Wright Nuclear Structure Laboratory, Yale University, New Haven, CT 06520.

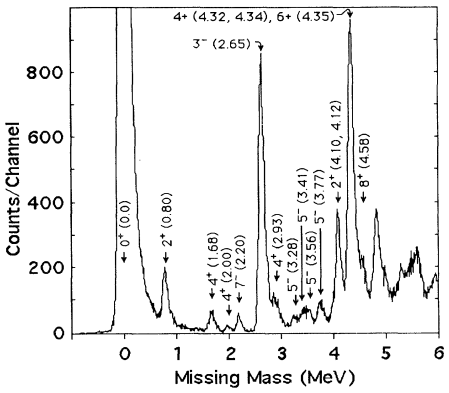

FIG. 1. Missing mass histogram for ^{206}Pb(p,p') at $T_p = 650$ MeV and $\theta_L = 16°$. Corresponding excitation energies in MeV are shown in parentheses.

$T_p = 650$ MeV in which the true 0° laboratory angle was established in spectrometer runs at 0° on the direct beam.

Absolute cross sections were determined by comparison of p-p scattering from a $(CH_2)_n$ target, using absolute p-p cross sections from the data base of Arndt and Roper [23], and are believed to be good to $\sim \pm 7\%$. Relative cross sections (elastic/inelastic) and 206/208, 207/208 ratios are expected to be good to $\sim \pm 3\%$.

The beam intensity was monitored by two ion chambers inside the target chamber. Beam polarization was measured in two ways: with an upstream ($\sim$ 5 m) CH_2 polarimeter and by the ion source quench method [24]. The two methods agreed to within 1%.

The standard LAMPF data acquisition system, "Q" [25] was used during the experiment and the subsequent off-line analysis. Two typical "missing mass" histograms generated by the Q system are shown in Figs. 1 and 2. The peak-fitting routine LOAF [26] was used to extract areas and centroids of the peaks of interest. Empirical line shapes were used in the peak fitting. Yields in each angle bin were corrected for chamber efficiency, system live time, and the nonuniformity of a solid angle across the horizontal direction (proportional to the scattering angle) in the focal plane. The beam current normalized and corrected yields were converted to absolute cross sections by comparing with p-p scattering as discussed above. The resulting cross sections (σ) and analyzing powers (A_y) are shown in Figs. 3–8.

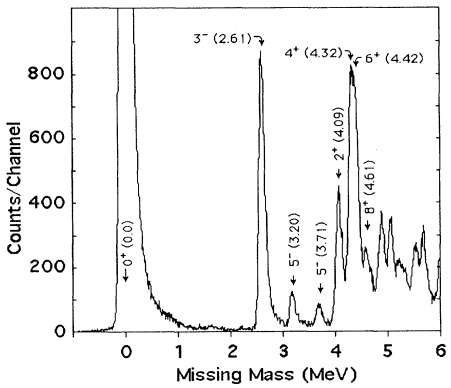

FIG. 2. Same as Fig. 1 except for ^{208}Pb.

III. ELASTIC-SCATTERING–OPTICAL-MODEL ANALYSIS

The elastic cross sections were fitted using the search program RELOM [27] with an optical potential of the form

$$U = Vf(x_R) + iWf(x_I) - (V_{SO} + iW_{SO})\frac{4}{r}f'(x_{SO})\vec{l}\cdot\vec{s} + V_c(r) ,$$

where

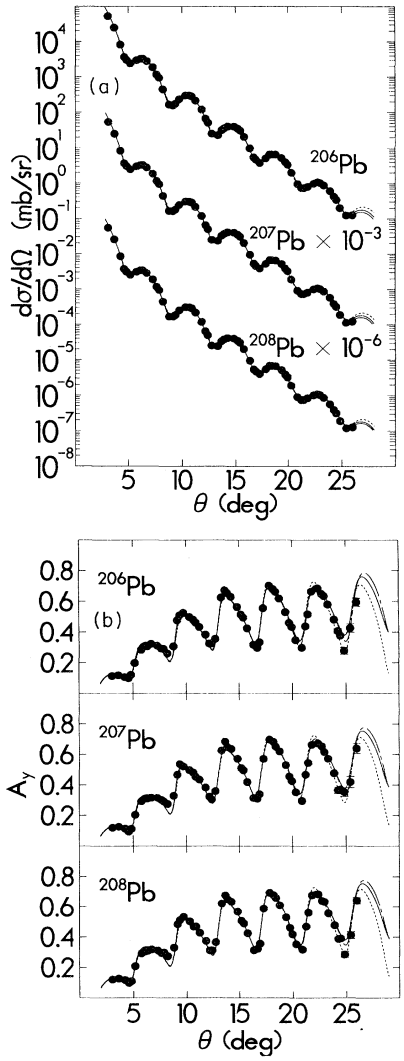

FIG. 3. (a) Elastic differential cross sections for proton scattering from ^{206,207,208}Pb at 650 MeV. The curves show optical-model predictions for potential sets I (solid), II (chain dashed), and III (dashed). (b) Same as for (a) except for elastic analyzing power.

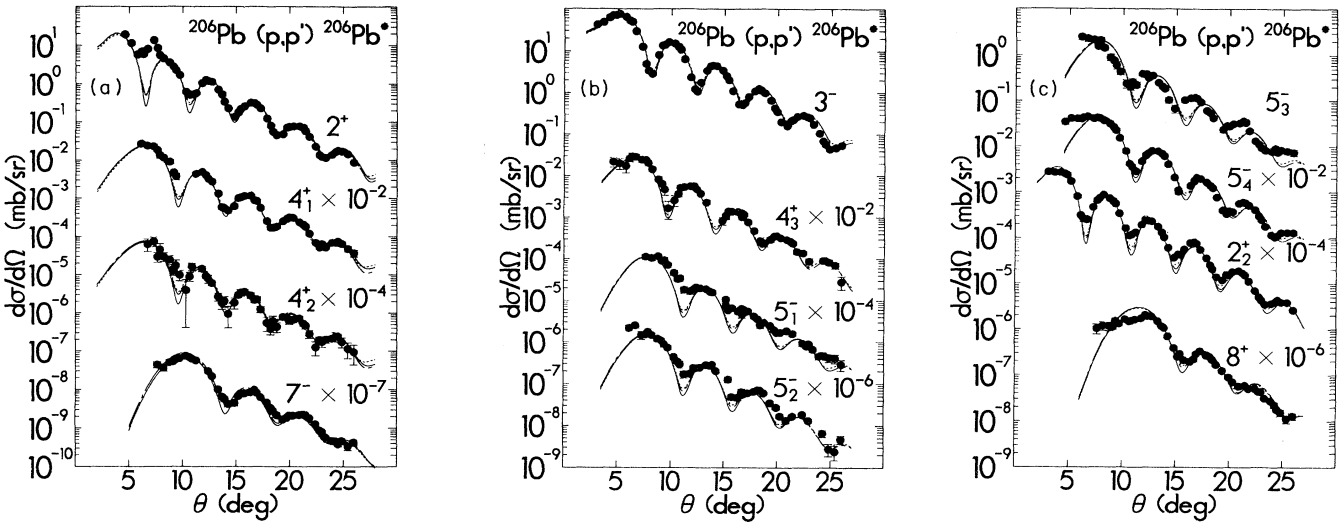

FIG. 4. Inelastic differential cross sections for ^{206}Pb(p,p') at 650 MeV. (a) For 2^+ (0.80 MeV), 4^+ (1.68 MeV), 4^+ (2.00 MeV), and 7^- (2.20 MeV) states. (b) For 3^- (2.65), 4^+ (2.93), 5^- (3.28), and 5^- (3.41) states. (c) For 5^- (3.56), 5^- (3.78), 2^+ (4.10), and 8^+ (4.58) states. The curves show vibrating-potential–collective-model fits from program ECIS. The solid, chain dashed, and dashed curves are from optical potential sets I, II, and III, respectively.

$$f(x) = \frac{1}{1+e^x}, \quad f' = \frac{d}{dr} f(x)$$

and

$$x_i = \frac{r - R_i}{a_i}, \quad i = R, I, SO \ . \tag{1}$$

The Coulomb potential $V_c(r)$ was assumed to be that of a uniformly charged sphere with $R_c = 1.0A^{1/3}$ fm. To facilitate comparison we write $R_i = r_i A^{1/3}$.

Five nearly equivalent classes of solution were found in the search procedure and are shown in Table I. These differ mainly in the real central parameters (V, r_R, and a_R), which the data clearly do not determine. Solution V has the lowest χ^2 but those for sets I–IV are not much higher. The optical-model predictions for parameter sets I–III are shown in Fig. 3 and are nearly indistinguishable from each other for angles $< 25°$. The results for sets IV and V are nearly identical to those for I–III. Set IV was generated with the real central potential, V, constrained to zero in the search.

Table II lists averages of the rms radii and volume integrals of the five sets for each isotope. The rms radii and volume integrals of the real central potential vary considerably among the five sets (from 3.6 to 8.5 fm for the radii and zero to $\sim$ 21 000 MeV fm^3 for the volume

TABLE I. Optical-model parameter sets. Potentials are in MeV, lengths in fm.

A	Set	V	r_R	a_R	W	r_I	a_I	V_{SO}	W_{SO}	r_{SO}	a_{SO}	χ^2	$\sigma_R(b)$
^{206}Pb	I	0.1311	1.8628	0.0019	−56.7576	1.0953	0.6083	−1.1169	−0.2234	1.0893	0.8380	184	1.7485
^{207}Pb	I	0.1324	1.8664	0.0023	−57.8896	1.0926	0.6132	−1.1649	0.2151	1.0831	0.8474	183	1.7592
^{208}Pb	I	0.1267	1.8777	0.0029	−59.3350	1.0886	0.6163	−1.1855	−0.2432	1.0784	0.8541	192	1.7655
^{206}Pb	II	64.3610	0.6868	0.4883	−75.3258	1.0535	0.6592	−1.2376	−0.1928	1.0713	0.8580	177	1.7987
^{207}Pb	II	60.7459	0.6921	0.5099	−74.5719	1.0553	0.6572	−1.2663	−0.1702	1.0686	0.8620	183	1.8023
^{208}Pb	II	74.7720	0.6559	0.5769	−75.7619	1.0524	0.6602	−1.2724	−0.1827	1.0673	0.8676	188	1.8087
^{206}Pb	III	1.9962	1.1843	0.0014	−64.4784	1.0724	0.6469	−1.1137	−0.1486	1.0945	0.8353	204	1.7776
^{207}Pb	III	1.9694	1.1780	0.0031	−64.0753	1.0739	0.6450	−1.1474	−0.1272	1.0905	0.8396	207	1.7823
^{208}Pb	III	1.7397	1.1798	0.0013	−64.7135	1.0727	0.6434	−1.1402	−0.1674	1.0893	0.8433	210	1.7853
^{206}Pb	IV	[0]			−61.5239	1.0835	0.6220	−1.2047	−0.2510	1.0740	0.8591	207	1.7616
^{207}Pb	IV	[0]			−61.2254	1.0844	0.6222	−1.2223	−0.2311	1.0731	0.8605	206	1.7677
^{208}Pb	IV	[0]			−62.3402	1.0815	0.6244	−1.2222	−0.2518	1.0723	0.8619	212	1.7738
^{206}Pb	V	23.6026	0.8177	0.4750	−64.4164	1.0782	0.6242	−1.1871	−0.2117	1.0743	0.8507	158	1.7645
^{207}Pb	V	23.2091	0.8248	0.4628	−65.5571	1.0759	0.6275	−1.2398	−0.1978	1.0677	0.8599	164	1.7737
^{208}Pb	V	20.7127	0.8597	0.4457	−66.3069	1.0748	0.6255	−1.2834	−0.2184	1.0594	0.8713	162	1.7769

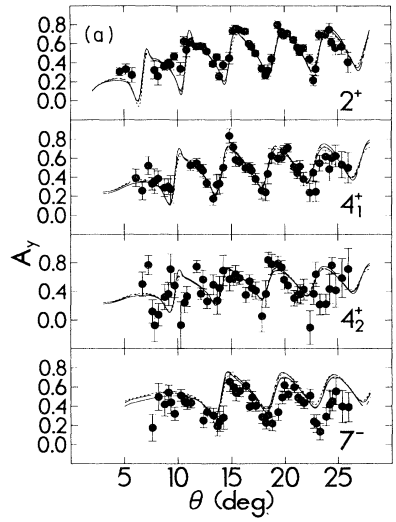

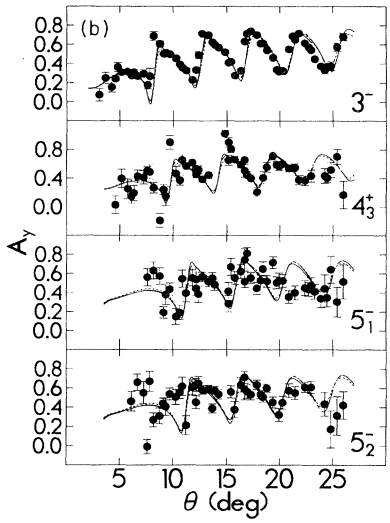

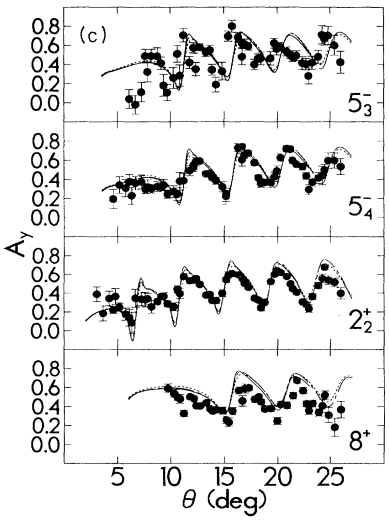

FIG. 5. Same as Fig. 4 but for inelastic analyzing power.

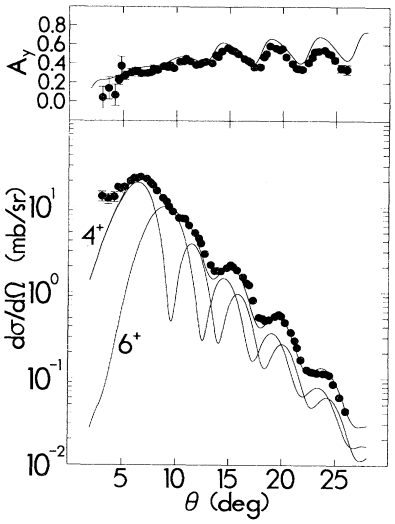

FIG. 6. Inelastic differential cross section and analyzing powers for unresolved 4^+ (4.32 MeV) and 6^+ (4.35 MeV) doublet in ^{206}Pb(p,p') at $T_p = 650$ MeV. The curves show collective-model predictions to 4^+ and 6^+ states and their sum. All curves are for potential set I, but the other sets give similar results.

integrals). However, the imaginary rms radii lie within a range of less than 1.5% and the imaginary central volume integrals within $\sim$ 15% for the five sets. Thus the imaginary rms radii, and to a lesser extent, the imaginary volume integrals are fairly well constrained by the data.

A feature which is strongly constrained by the data is the magnitude of $W(r)$ in the nuclear surface, as was discovered long ago for strongly absorbed projectiles [28]. For $r >\sim 6.5$ fm, values of $W(r)$ differ by $< 4\%$ for the five potential sets even though the central values are spread by almost 30%.

To explore further the accuracy with which the data determine the rms radii of the imaginary central potential we have done a sequence of optical potential searches, in each of which the rms radius (of the central imaginary potential) is fixed (which couples r_I and a_I), but allowing the remaining eight parameters to vary freely. This sequence of searches generates the curves shown in Fig. 9 which display χ^2 vs $\langle r^2\rangle^{1/2}$. The curves differ slightly depending on which parameter set is used as the starting point for the searches, but this procedure indicates that the rms radii are determined to within about $\pm$ 0.1 fm by the data.

To compare our phenomenological rms radii and volume integrals with those expected for potentials, $U(r)$, obtained in the first-order impulse approximation (IA) we can write

$$U(r) = \sum_{i=n,p} \int \rho_i(r) t_i(|\vec{r} - \vec{r}'|) d^3r' \ ,$$

where $\rho_i(r)$ is the one-body nucleon density and t_i the free nucleon-nucleus t matrix. If we define the volume

integrals

$$J_0(h) = \int h(r) d^3\vec{r} \,, \tag{2}$$

we can use the theorems of Satchler [29] to write

$$J_0(U_i) = J_0(\rho_i) J_0(t_i) = N_i J_0(t_i), \quad i : n, p \tag{3}$$

where

$$N_p = Z \text{ and } N_n = N$$

and also

$$\langle r^2 \rangle_{U_i} = \langle r^2 \rangle_{\rho_i} + \langle r^2 \rangle_{t_i} \tag{4}$$

for the mean-square radii. Then for the optical potential we expect

$$U = U_n + U_p \tag{5}$$

and

$$\langle r^2 \rangle_U = \frac{J_0(U_p)\langle r^2 \rangle_{U_p} + J_0(U_n)\langle r^2 \rangle_{U_n}}{J_0(U)} \,. \tag{6}$$

For a Woods-Saxon potential [Eq. (1)] the volume integrals and mean-square radii can be calculated with sufficient accuracy [30] from

$$J_0(U_i) = U_i \frac{4\pi}{3} R_i^3 \left[1 + \left(\frac{\pi a_i}{R_i}\right)^2\right] \tag{7}$$

and

$$\langle r_i^2 \rangle = 3/5 R_i^2 \left[1 + 7/3 \left(\frac{\pi a_i}{R_i}\right)^2\right] \,. \tag{8}$$

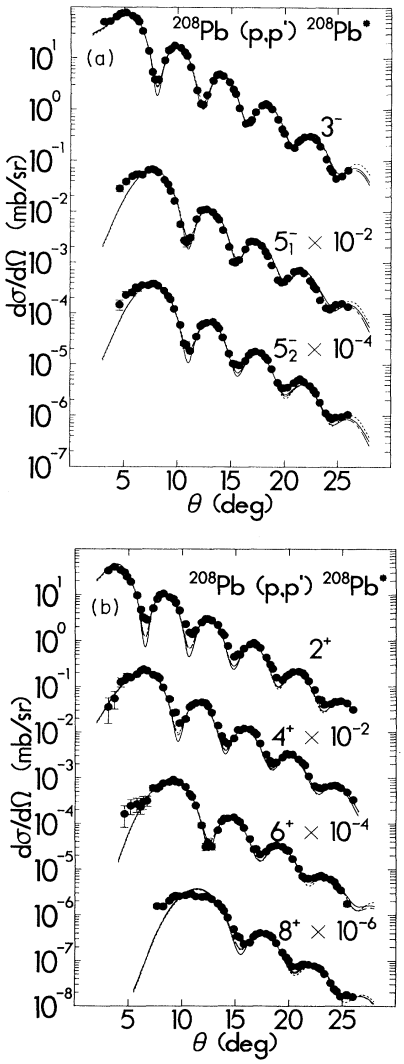

FIG. 7. Inelastic differential cross sections for ^{208}Pb(p,p') at $T_p = 650$ MeV. (a) For 3^- (2.61), 5^- (3.20), and 5^- (3.71) states. (b) For 2^+ (4.09), 4^+ (4.32), 6^+ (4.42), and 8^+ (4.61) states. The curves are collective model predictions with the same legend as in Fig. 4.

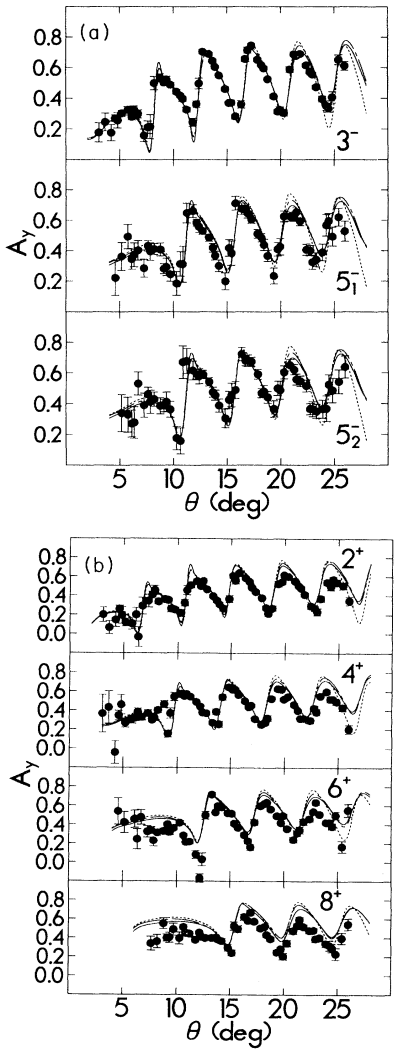

FIG. 8. Same as Fig. 7 but for inelastic analyzing power.

TABLE II. Comparisons of volume integrals, J_0, and root-mean-square radii $\langle r^2\rangle^{1/2}$ for (central) optical-potential (average, AV, of sets I–V) with values for the impulse approximation (IA) from folding theorems using the Franey-Love interaction (including exchange). R, real; I, imaginary.

	206		207		208	
	AV[a]	IA	AV[a]	IA	AV[a]	IA
$\langle r^2\rangle_R^{1/2}$	5.4 ± 2	$4.25i$[b]	5.5 ± 2	$3.97i$[b]	5.5 ± 2	$3.70i$[b]
$\langle r^2\rangle_I^{1/2}$	5.46 ± 0.03	5.63	5.47 ± 0.03	5.64	5.46 ± 0.03	5.65
fm						
J_0^R	$9\,089 \pm 7906$	1387	$8\,992 \pm 7\,771$	1457	$9\,484 \pm 8\,660$	1528
MeV f,^{3}						
J_0^I	$-76\,035$	$-84\,986$	$-76\,593$	$-85\,378$	$-77\,698$	$-85\,770$
MeV f,^{3}	± 4735		$\pm 4\,383$		$\pm 4\,324$	

[a]Showing rms deviations of sets I–V values from the average value.
[b]$\langle r^2\rangle_R$ is negative.

Comparisons of the values for the impulse approximation from Eqs. (2)–(8) with averages for the phenomenological potentials are shown in Table II where the Franey-Love interaction including exchange [31] was used for t_i. It is seen that the imaginary central volume integrals, for which comparisons are most meaningful, are close to those of the IA, but systematically 10–20 % lower in magnitude (except for set II which is equal to the IA value). The rms imaginary radii, which are determined by the data to within $\sim$ 1%, are consistently $\sim$ 3% smaller than those for the IA potentials. This is another example of the "radius problem" with the nonrelativistic IA [32]. The problem persists even for comparatively sophisticated nonrelativistic theories such as the coupled-channels isobar model of Ray [33] in which conventional medium modifications are included. We believe this problem can be at least partially fixed by allowing a reduction of meson and nucleon masses in the nuclear medium. This effect modifies the N-N interaction in a density-dependent manner [32].

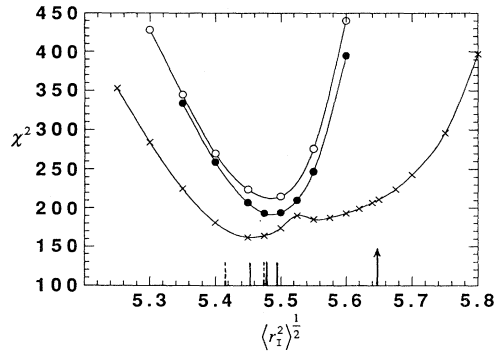

FIG. 9. Values of χ^2 vs $\langle r_I^2\rangle^{1/2}$ (constrained in search) for ^{208}Pb with starting points in search set I (solid circles), set IV (open circles), and set V (crosses) parameters. Short vertical solid lines indicate χ^2 minima for sets I, IV, and V. Short vertical dashed lines show location of minima for sets II and III. The vertical arrow indicates value of $\langle r_I^2\rangle^{1/2}$ predicted by the impulse approximation with the FL interaction.

Comparison of the rms radii and volume integrals of the central real potential are not very meaningful since the potential is not determined by the data, and the IA gives negative values for $\langle r^2\rangle_R$, which cannot occur for any potentials of the Woods-Saxon shape. It is known that in relativistic [34] or medium modified nonrelativistic IA treatments [33,35] the real central potential is considerably altered, but the imaginary only slightly, in comparison to the nonrelativistic IA with the free t matrix, especially at energies above 500 MeV.

IV. INELASTIC-SCATTERING–VIBRATING-POTENTIAL MODEL

A. Deformation lengths

In the vibrating potential model (VPM) or "collective model," the radial part of the inelastic transition potential can be written in terms of the elastic potential, U,

$$U_{\rm tr} = \beta_\lambda R \frac{\partial U}{\partial r} \equiv \delta_U U' \ . \tag{9}$$

To determine δ_U, the program ECIS [36] was used. The same deformation parameters, β_λ, were used for all parts of the optical potential. The VPM predictions together with the data for ^{206,208}Pb are shown in Figs. 4–8. Average values for potential sets I–V of the β_λ and δ_U for the central imaginary potential, which dominates, are given in Table III. The values of δ_U for the individual potential sets lie within $\sim$ 1% of their averages. For the unresolved 4^+ (4.32 MeV) and 6^+ (4.35 MeV) states of ^{206}Pb, shown in Fig. 6, the data were fit with a sum of $\lambda = 4$ and 6 vibrations. The fits are seen to be very good for most of the cross section, σ, and analyzing power, A_y, data. An analysis of the ^{207}Pb inelastic data will appear in a later paper.

B. Neutron-proton matrix element ratios

To obtain separate neutron and proton transition matrix elements from the potential deformation, lengths, δ_U,

TABLE III. Average imaginary deformation parameters β_λ and deformation lengths, $\delta_U = \beta_\lambda R_I$, for optical potential sets I–V.

Nucleus	λ^π	E_{ex} MeV	β_λ	δ_U (fm)
^{206}Pb	2^+	0.80	0.0468	0.296
	4^+	1.68	0.0285	0.180
	4^+	2.00	0.0147	0.0931
	7^-	2.20	0.0253	0.160
	3^-	2.65	0.126	0.794
	4^+	2.93	0.0305	0.193
	5^-	3.28	0.0236	0.149
	5^-	3.41	0.0274	0.173
	5^-	3.56	0.0316	0.200
	5^-	3.78	0.0478	0.302
	2^+	4.10	0.0649	0.410
	4^+	4.32	0.0819	0.517
	6^+	4.35	0.0766	0.484
	8^+	4.58	0.0579	0.366
^{208}Pb	3^-	2.61	0.128	0.812
	5^-	3.20	0.0568	0.360
	5^-	3.71	0.0431	0.273
	2^+	4.09	0.0709	0.448
	4^+	4.32	0.0865	0.548
	6^+	4.42	0.0758	0.480
	8^+	4.61	0.0633	0.401

and electromagnetic data, it is necessary to make certain approximations [37], which we note below. We use here a slightly refined version of the methods described in [3,4]. The main assumptions are the first-order IA and simple derivative forms for both the interaction potential [Eq. (9)] and the transition densities [Eq. (14)], not necessarily of the same shape. The latter assumption is somewhat inconsistent [37] but is used only to derive *ratios* of geometric quantities.

In the IA the elastic optical potential, U, can be decomposed into neutron and proton contributions,

$$U = U_n + U_p \ , \tag{10}$$

thus

$$U_{\rm tr} = \delta_U U' = \delta_U (U'_n + U'_p) = U_n^{\rm tr} + U_p^{\rm tr} \ . \tag{11}$$

We then assume that the $U_i^{\rm tr}$ $(i : n, p, q)$ can be obtained by folding the ground-state density derivatives ρ'_i multiplied by δ_i, with the two-body interactions, t_{pi}. Satchler's theorem [29] for multipole moments states that for a function $h(r)$ obtained by folding $f(r')$ with $t(|r - r'|)$ that

$$J_\lambda(h) = J_\lambda(f) J_0(t) \ , \tag{12}$$

where

$$J_\lambda(f) = 4\pi \int_0^\infty r^{\lambda+2} f(r) dr \ . \tag{13}$$

Then from Eqs. (11) and (12) we obtain

$$\delta_U [J_\lambda(U'_n) + J_\lambda(U'_p)] = \delta_n J_\lambda(\rho'_n) J_0(t_{pn}) + \delta_p J_\lambda(\rho'_p) J_0(t_{pp}) \ , \tag{14}$$

we now use $J_\lambda(f') = -(\lambda + 2)\langle r^{\lambda-1}\rangle_f J_0(f)$ and define $\epsilon_f = \langle r^{\lambda-1}\rangle_f$ where the $\langle r^{\lambda-1}\rangle_f$ are the average values of $r^{\lambda-1}$ for the function f. We also assume that U_i results from folding ρ_i with t_{pi} so that Eq. (12) applies.

This gives $(\epsilon_{\rho_i} = \epsilon_i)$

$$\delta_U [\epsilon_{U_n} N J_0(t_{pn}) + \epsilon_{U_p} Z J_0(t_{pp})] = \delta_n \epsilon_n N J_0(t_{pn}) + \delta_p \epsilon_p Z J_0(t_{pp}) \ . \tag{15}$$

Defining

$$C \equiv \frac{Z J_0(t_{pp})}{N J_0(t_{pn})} \ , \tag{16}$$

we have the final result

$$\delta_n = \frac{1}{\epsilon_n} [\delta_U (\epsilon_{U_n} + C \epsilon_{U_p}) - \delta_p \epsilon_p C] \ . \tag{17}$$

The reduced (N or Z factors removed) transition matrix elements are defined as

$$\tilde{M}_i(\lambda) = \frac{1}{N \text{ or } Z} \int_0^\infty \rho_i^{\rm tr} r^{\lambda+2} dr = \left(\frac{\lambda + 2}{4\pi} \langle r^{\lambda-1}\rangle_i \delta_i \right) \tag{18}$$

in our case. Thus from Eqs. (17) and (18) we find

$$\tilde{M}_n / \tilde{M}_p = \frac{\delta_n \epsilon_n}{\delta_p \epsilon_p} = \frac{\epsilon_{U_n} + C \epsilon_{U_p}}{\delta_q \epsilon_q} - C \ , \tag{19}$$

where we have used the equality of charge (q) and point density moments [29]. Note that we have improved on the usual assumption that $\delta_{U_i} = \delta_i$ and $\delta_p = \delta_q$ but have instead used the equality of the J_λ multipole moments.

In Eqs. (17) and (19) we have reduced the problem of separating the neutron and proton deformation lengths to that of evaluating ratios of moments of the $U_{n,p}$, $\rho_{n,p,q}$ and the interaction strengths.

To obtain the density moments ϵ_i for ^{208}Pb we have used the ground-state densities of [9,38–40] adjusted slightly for ρ_n and ρ_p to agree with the rms neutron and proton radii obtained in our recent analysis of the ^{206,208}Pb elastic scattering data at 650 MeV [17]. In the scaling we have assumed that $\langle r^n\rangle$ scales as $\langle r^2\rangle^{n/2}$.

The moments of U_p and U_n were derived from the moments of the phenomenological potential, U (set I, closest to the folded geometry) assuming that the U_n and U_p moments are in the same ratio as expected from folding. The potential and density moments used are given in Table IV.

To calculate C the Franey-Love interaction at 650 MeV [31], including exchange, was employed. The values of C are also given in Table IV.

The moments for ^{206}Pb were obtained by scaling those of ^{208}Pb, again as $\langle r^2\rangle^{n/2}$. These are also given in Table IV. The values of δ_p and δ_q are derived from reduced

TABLE IV. Radial moments $\langle r^n \rangle_i$ used in calculation of $\tilde{M}_n/\tilde{M}_p$.

	n					
	1	2	3	4	5	7
^{206}Pb						
ρ_q[a]	5.267	30.122	182.77			
ρ_n	5.384	31.551	196.70			
ρ_p	5.235	29.648	177.46			
U_n	5.319	31.030	193.80			
U_p	5.175	29.136	174.53			
^{208}Pb						
ρ_q	5.280	30.265	184.07	1 173.3	7 780	378 459
ρ_n	5.414	31.900	199.97	1 317.3	9 053	476 855
ρ_p	5.248	29.790	178.74	1 119.6	7 268	333 015
U_n	5.315	31.012	193.82	1 282.9	8 933	497 587
U_p	5.171	29.119	174.55	1 099.2	7 218	348 523

$C = 0.7480(^{206}\text{Pb}), 0.7361\ (^{208}\text{Pb})$

[a]The charge moments, δ_q, for ^{208}Pb were calculated with the $3PG$ of [41]. Those for ^{206}Pb were obtained by scaling as described in the text.

electromagnetic transition rates and

$$\delta_p \langle r^{\lambda-1} \rangle_p = \delta_q \langle r^{\lambda-1} \rangle_q \ , \tag{20}$$

where

$$B(E\lambda) = |Z\tilde{M}_q(\lambda)|^2 = \left(\frac{Z(\lambda+2)}{4\pi} \langle r^{\lambda-1} \rangle_q \delta_q \right)^2 . \tag{21}$$

The adopted $B(E\lambda)$'s for ^{208}Pb were taken from [3] except for the $B(E3)$ for the 3_1^- (2.61 MeV) where we have used the adopted value from [10], i.e., $B(E3) = 0.611(9)$ $e^2\text{b}^3$. For ^{206}Pb we have used the $B(E\lambda)$ given in [8,10]. Our values of δ_U, δ_n, and $\tilde{M}_n/\tilde{M}_p$ are given in Table V along with the $B(E\lambda)$ and δ_p used, as well as earlier values of $\tilde{M}_n\tilde{M}_p$.

In Table VI we compare the absolute values of M_n and M_p (N or Z factors included) and the ratios $\tilde{M}_n/\tilde{M}_p$ with the RPA calculations of Decharge [13,14] for ^{208}Pb and our recent RPA predictions for ^{206}Pb [19].

V. SUMMARY AND CONCLUSIONS

We have presented data for the elastic and inelastic scattering of 650-MeV protons by ^{206,207,208}Pb. Five phenomenological Woods-Saxon optical-model potential sets were found by searching on the elastic cross section and analyzing power data. The potential volume integrals (J_0) and mean-square radii were compared with those expected from the impulse (or "$t\rho$") approximation (IA). The correspondence is not meaningful for the real central potential which is poorly determined. For the imaginary central potential the phenomenological volume integrals are close to, but systematically $\sim$ 5–10% lower (except for set II) than those from the IA. The rms radii for the phenomenological imaginary central potentials are also $\sim$ 3% smaller than the IA values, which is consistent with the "shrinking" of the effective potential, at least for the real parts, predicted by Brown *et al.* as a consequence of the reduction of meson and nucleon masses in the nuclear medium [32]. Most of the difference be-

TABLE V. Reduced neutron-proton matrix element ratios $\tilde{M}_n/\tilde{M}_p$ for ^{206,208}Pb and input data for calculation.

Nucleus	J^π	E_{ex} (MeV)	δ_U (fm)	$B(E\lambda)$[a] ($e^2\text{b}^\lambda$)	δ_p (fm)	δ_n (fm)	$\tilde{M}_n/\tilde{M}_p$ This[b]	$\tilde{M}_n/\tilde{M}_p$ Other[c] p/e		π^+/π^-
										[f]
^{206}Pb	2^+	0.80	0.296	0.099(4)	0.2303	0.3377	1.51(5)			1.65(11)
	4^+	1.68	0.180	0.0167	0.1860	0.1713	1.02			
	3^-	2.65	0.794	0.62(5)	0.8140	0.7572	0.99(7)			1.00 (7)
	2^+	4.10	0.410	0.23(2)	0.3510	0.4445	1.30(9)			1.00 (7)
	4^+	4.32	0.517	0.22(2)	0.6751	0.3970	0.65(7)			
								[d]	[e]	
^{208}Pb	3^-	2.61	0.812	0.611(9)	0.8042	0.7822	1.04(2)	1.13[d]	0.97[e]	1.12
	5^-	3.20	0.360	0.0447(30)	0.4134	0.3131	0.89(6)	1.23	0.97	1.32
	5^-	3.71	0.273	0.0241(18)	0.3036	0.2436	0.94(7)	1.11	0.82	1.15
	2^+	4.09	0.448	0.318(16)	0.4117	0.4611	1.16(5)	1.30	0.95	1.13
	4^+	4.32	0.548	0.155(11)	0.5626	0.5131	1.02(7)	1.13	0.92	1.00
	6^+	4.42	0.480	0.0665(67)	0.6797	0.3537	0.65(8)	0.93	0.70	1.08
	8^+	4.61	0.401	0.0054(9)	0.3382	0.4603	1.95(27)	1.60	1.12	1.54

[a]Error in last digits given in parentheses.
[b]In parentheses: error in last digits due only to uncertainty in $B(E\lambda)$.
[c]See [2,4] for references.
[d]Average of values from T_p = 500 and 800 MeV. See [4].
[e]Average of values from T_p = 35–400 MeV. See [4].
[f]Average of values from T_π = 116–291 MeV. See Refs. [2,42].

TABLE VI. Comparison of neutron and proton transition matrix elements with RPA predictions.

Nucleus	J^π	E_x	This			RPA[a]		
		MeV	M_n	M_p	$\tilde{M}_n/\tilde{M}_p$	M_n	M_p	$\tilde{M}_n/\tilde{M}_p$
			$eb^{\lambda/2}$			$eb^{\lambda/2}$		
^{206}Pb	2^+	0.80	0.718	0.315	1.51	0.508	0.282	1.19
	4^+	1.68	0.199	0.129	1.02	0.179	0.115	1.03
	3^-	2.65	1.179	0.787	0.99	1.0247	0.777	0.87
	2^+	4.10	0.945	0.480	1.30	0.604	0.470	0.85
^{208}Pb	3^-	2.61	1.251	0.782	1.04	1.230	0.798	1.00
	5^-	3.20	0.289	0.211	0.89	0.378	0.200	1.23
	5^-	3.71	0.225	0.155	0.94	0.132	0.124	0.69
	2^+	4.09	1.001	0.564	1.16	0.781	0.545	0.93
	4^+	4.32	0.617	0.394	1.02	0.489	0.351	0.91
	6^+	4.42	0.257	0.258	0.65	0.184	0.141	0.85

[a]From [19] for ^{206}Pb and [13,14] for ^{208}Pb.

tween the empirical imaginary central potential volume integrals and the IA values is thus due to the smaller empirical rms radii, indicating that the imaginary potential strengths themselves are close to the IA values.

The inelastic cross sections and analyzing powers for ^{206,208}Pb were analyzed with collective form factors derived from the elastic optical potential. The agreement with experiment is generally quite good. From the potential deformation lengths, given by the normalization of the collective model predictions to the data, and charge deformation lengths from electron scattering, neutron-proton transition matrix element ratios were calculated. The values reported here for ^{208}Pb, except for the 8^+ state, mostly lie between the averages for low-energy (T_p = 35–400 MeV) and high-energy (T_p = 500 and 800 MeV) e/p determinations, and thus are consistent with the slight energy dependence ($\tilde{M}_n/\tilde{M}_p$ decreasing slightly with T_p) found in the global analysis of [4]. They are also in rough ($\sim \pm 10\%$) agreement with those from π^+/π^- comparisons except for the 5^-, 6^+, and 8^+ states.

For ^{206}Pb there are only a few $B(E\lambda)$'s available so $\tilde{M}_n/\tilde{M}_p$ could be obtained for only five states. Only the 2^+ (0.80 MeV) and 2^+ (4.10 MeV) states have the values of $\tilde{M}_n/\tilde{M}_p$ significantly larger than unity as would be expected for a two-neutron-hole configuration. The summed strength ($\Sigma\delta_U^2$) for each multipole in ^{206}Pb is comparable (within $\sim$ 10–15%) of the corresponding sum for ^{208}Pb, except for $\lambda^\pi = 2^+$ for which it is 27% greater.

The absolute values of M_n and M_p from this work are generally in rough agreement with RPA predictions but on the average $\sim$ 20% higher. There is no systematic pattern to the ratios, $\tilde{M}_n$ $\tilde{M}_p$ but the RPA values are within $\pm$35% or less of our results.

In a recent paper [17] we presented a model-independent analysis of the elastic scattering data, using an effective N-N interaction, to obtain ground-state neutron densities. A microscopic analysis of the inelastic data is given in [19].

ACKNOWLEDGMENTS

We wish to thank the staff of the Los Alamos Meson Physics Facility, particularly John McClelland and Kevin Jones for the many hours spent in assisting this experiment. This work was supported by the U.S. Department of Energy and the Robert A. Welch Foundation.

[1] C. Olmer, D. F. Geesaman, B. Zeidman, S. Chakravarti, T.-S. H. Lee, R. L. Boudrie, R. H. Siemssen, J. F. Amann, C. L. Morris, H. A. Theissen, G. R. Burleson, M. J. Devereux, R. E. Segel, and L. W. Swenson, Phys. Rev. C **21**, 254 (1980).

[2] N. M. Hintz, X. H. Yang, M. Gazzaly, S. J. Seestrom-Morris, C. L. Morris, D. C. Cook, A. M. Mack, J. W. McDonald, S. Mordechai, D. S. Oakley, C. F. Moore, M. Lynker, and J. D. Zumbro, Phys. Rev. C **45**, 601 (1992), and references therein.

[3] M. M. Gazzaly, N. M. Hintz, G. S. Kyle, R. K. Owen, G. W. Hoffmann, M. Barlett, and G. Blanpied, Phys. Rev. C **25**, 408 (1982).

[4] Norton M. Hintz, D. Cook, M. Gazzlay, M. A. Franey, M. L. Barlett, G. W. Hoffmann, R. Fergerson, J. McGill, G. Pauletta, R. L. Boudrie, J. B. McClelland, and K. Jones, Phys. Rev. C **37**, 692 (1988).

[5] D. J. Horen, R. L. Auble, J. R. Beene, F. E. Bertrand, M. L. Halbert, G. R. Satchler, M. Thoennessen, R. L. Varner, V. R. Brown, P. L. Anthony, and V. A. Madsen, Phys. Rev. C **44**, 128 (1991).

[6] B. Frois, J. B. Bellicard, J. M. Cavedon, M. Huet, P. Leconte, P. Ludeau, A. Nakada, Phan Zuan Hò, and I. Sick, Phys. Rev. Lett. **38**, 152 (1977).

[7] J. Heisenberg, J. Lichtenstadt, C. N. Papanicolas, and J. S. McCarthy, Phys. Rev. C **25**, 2292 (1982); J. Heisenberg, *Advances in Nuclear Physics* (Plenum, New York, 1981), Vol. 12, p. 61. See also [3] for other ^{208}Pb (e, e') references and adopted $B(E\lambda)$ values used here.
[8] C. N. Papanicolas, J. Heisenberg, J. Lichtenstadt, J. S. McCarthy, D. Goutte, J. M. Cavedon, B. Frois, M. Huet, P. Leconte, Phan Xuan Hò, S. Platchkov, and I. Sick, Phys. Rev. Lett. **52**, 247 (1984); C. N. Papanicolas, Ph.D. thesis, Massachusetts Institute of Technology, 1979 (unpublished).
[9] H. de Vries, C. W. de Jager, and C. de Vries, At. Data Nucl. Data Sheets **36**, 495 (1987).
[10] R. G. Helmer and M. A. Lee, Nucl. Data Sheets **61**, 93 (1990).
[11] V. Gillet, A. M. Green, and A. M. Sanderson, Nucl. Phys. **88**, 321 (1966).
[12] P. Ring and J. Speth, Nucl. Phys. **A235**, 315 (1974).
[13] J. Decharge, M. Girod, D. Gogny, and B. Grammaticos, Nucl. Phys. **A358**, 203C (1981); J. Decharge and D. Gogny, Phys. Rev. C **21**, 1568 (1980).
[14] J. Decharge, Centre d'Etudes de Bruyeres-le-Chatel Report CEA-N-2260, 1982 (unpublished); J. Decharge (private communication).
[15] See, for example, [6] and references therein for ^{208}Pb.
[16] S. E. Frolking, M.A. thesis, University of New Hampshire, 1980 (unpublished).
[17] V. E. Starodubsky and N. M. Hintz, Phys. Rev. C **49**, 2118 (1994).
[18] V. E. Starodubsky and N. M. Hintz, Phys. Rev. C **49**, 2479 (1994).
[19] V. E. Starodubsky and Norton Hintz, J. Phys. G **21**, 803 (1995).
[20] B. Zeidman, Los Alamos National Laboratory Report LA-4773-MS, 1971 (unpublished).
[21] C. L. Morris, H. A. Thiessen, and G. W. Hoffmann, IEEE Trans. Nucl. Sci. **NS-25**, 141 (1978).
[22] G. W. Hoffman *et al.*, "Nuclear Structure Studies using the HRS at LAMPF," University of Texas Annual Progress report, 1984 (unpublished), p. 101.
[23] R. A. Arndt and D. Roper, VPI and SU Scattering Analysis Interaction Dial in Nucleon-Nucleon Program (unpublished).
[24] M. W. McNaughton, P. R. Bevington, H. B. Willard, E. Winkelmann, E. P. Chamberlin, F. H. Cverna, N. S. P. King, and H. Willmes, Phys. Rev. C **23**, 1128 (1981).
[25] J. F. Harrison *et al.*, IEEE Trans. Nucl. Sci. **NS-28**, 3724 (1981).
[26] L. E. Smith, Computer code LOAF, 1983 (unpublished).
[27] G. J. Pyle, Computer code RAROMP, University of Minnesota Informal Report COO-1265-64, 1964 (unpublished) modified for relativistic energies.
[28] G. Igo, Phys. Rev. Lett. **1**, 72 (1958).
[29] G. R. Satchler, J. Math. Phys. **13**, 1118 (1972).
[30] A. Bohr and B. R. Mottelson, *Nuclear Structure* (Benjamin, New York, 1969), Vol. I, p. 160.
[31] M. A. Franey and W. G. Love, Phys. Rev. C **31**, 488 (1985).
[32] G. E. Brown, A. Sethi, and N. M. Hintz, Phys. Rev. C **44**, 2653 (1991).
[33] L. Ray, Phys. Rev. C **41**, 2816 (1990), see Fig. 17.
[34] J. J. Kelly and S. J. Wallace, Phys. Rev. C **49**, 1315 (1994).
[35] See, for example, B. S. Flanders *et al.*, Phys. Rev. C **43**, 2103 (1991), Fig. 15
[36] J. Raynal, Computer Code ECIS, 1979 (unpublished).
[37] See G. R. Satchler, Phys. Rev. C **50**, 317 (1994), for a critical discussion of this problem.
[38] L. Ray, W. R. Coker, and G. W. Hoffmann, Phys. Rev. C **18**, 2641 (1978).
[39] G. W. Hoffmann *et al.*, Phys. Rev. C **21**, 1488 (1980).
[40] L. Ray, Phys. Rev. C **19**, 1855 (1979).
[41] C. W. DeJager, H. DeVries, and C. DeVries, Nucl. Data Sheets **14**, 479 (1974).
[42] R. J. Peterson, Phys. Rev. C **48**, 1128 (1993).